Electronic Supplementary Material (ESI) for Energy & Environmental Science.

Electronic Supplementary Information

Solvent-controlled O_2 diffusion enables air-tolerant solar hydrogen generation

Michael G. Allan,[a] Morgan J. McKee,[a] Frank Marken,[b] and Moritz F. Kuehnel*[a,c]

[a] Department of Chemistry, Swansea University, Singleton Park, Swansea SA2 8PP, UK

[b] Department of Chemistry, University of Bath, Claverton Down, Bath BA2 7AY, UK

[c] Fraunhofer Institute for Microstructure of Materials and Systems IMWS, Walter-Hülse-Straße 1, 06120 Halle, Germany

* Corresponding author email address: m.f.kuehnel@swansea.ac.uk

Experimental section

Methods

Chemical Reagents. Choline chloride (>99%), urea (analytical grade, 99.5%), ethylene glycol (>99%), glycerol (>99%), dicyandiamide (DCDA, 99%), potassium thiocyanate, triethanolamine (>98%), dihydrogen hexachloroplatinate hexahydrate, methyl viologen dichloride hydrate (>98%), methylene blue (>82%) and sodium chloride (laboratory grade, extra pure) were purchased from Fisher Scientific and used without further purification. 18.2 mΩ water was used throughout the work. Pt colloids (nanoparticle suspension, 1000 mg L^{-1}), potassium hexacyanoferrate(II) trihydrate (98.5-102.0%), TiO_2 (Aeroxide P25) and Eosin Y (disodium salt, dye content >85%) were purchased from Sigma Aldrich. Fresh seawater was collected from Swansea Bay, Swansea on 27th July 2021 at 17:30.

Synthesis of $^{NCN}CN_x$ Graphitic carbon nitride was synthesised according to a literature procedure, whereby DCDA (5 g) was weighed into an alumina crucible, covered, and then heated in a muffle furnace at 550°C in air for 4 hours (10°C min^{-1}).[1] After cooling to room temperature, the yellow mass denoted DCDA-CN_x was thoroughly ground in a mortar and pestle (2.33 g). $^{NCN}CN_x$ was synthesised according to a slightly modified literature procedure.[2] DCDA-CN_x (1.0 g) was ground in a mortar and pestle with KSCN (2.0 g). The yellow powder was then dried overnight under vacuum at 140°C, before being placed in an open alumina crucible followed by heating in a muffle furnace to 400°C for 1 hour (10°C min^{-1}) under N_2 (4 L min^{-1}) and a further heating step under N_2 at 500°C for 30 minutes (10°C min^{-1}). An olive-green mass remained after cooling to room temperature, which was ground in a mortar and pestle, followed by tip sonication in a phosphate buffer for 10 minutes (0.1 M, pH 4.5). The resulting suspension was filtered and washed with water and ethanol, and the solid was collected and then dried under vacuum overnight at 50°C (0.76 g). DR UV-Vis shows an absorption edge around 450 nm for both DCDA-CN_x and $^{NCN}CN_x$, corresponding to a band gap of 2.76 eV (Figure S1). Cyanamide functionalisation gives rise to a characteristic band at 2180 cm^{-1} in the FT-IR spectrum (Figure S2). PXRD (Figure S3) showed a decrease in the inter-layer spacing from 3.35 Å (2θ=26.55°) to 3.18 Å (2θ=27.96°) as previously reported.[2, 3]

Synthesis of Deep Eutectic Solvents (DESs). *Reline, glyceline* and *ethaline* were prepared in accordance with literature procedures[4, 5] by stirring choline chloride with urea, glycerol and ethylene glycol, respectively in a 1:2 molar ratio at 80°C until a homogenous liquid had formed.

Photocatalytic H_2 Generation in DESs. $^{NCN}CN_x$ (2.0 mg, unless otherwise stated) was transferred into a glass sample vial (Chromacol 10-SV, Fisher) along with the reagent solution (2.0 mL unless otherwise stated, see Tables S1, S3, S6 for conditions). Samples were capped with rubber septa and agitated in a sonic bath for 20 minutes. Samples analysed under N_2 were purged for 10 minutes prior to irradiation to de-aerate the solution. Samples were irradiated using a solar light simulator (Thermo Oriel 92194-1000) equipped with an AM 1.5G filter (Newport) with an intensity of 1 sun. Samples were mounted in a water bath maintained at 40°C and stirred at 800 RPM. The sample headspace was subject

to a constant purge of N_2 or air at a rate of 4 mL min^{-1} controlled by a mass flow controller (Bronkhorst). H_2 evolution was monitored by gas chromatography (Shimadzu Nexis 2030) using an auto-sampler programmed to inject 2 mL of the selected headspace stream. Experiments using TiO_2 and Eosin Y were performed in the same manner using TiO_2 (2 mg) and Eosin Y (2 mM) instead of $^{NCN}CN_x$.

Co-catalyst attachment experiments. Photocatalytic H_2 generation was performed by the standard procedure in reline (2.0 mg $^{NCN}CN_x$, 0.05 mg Pt as H_2PtCl_6, 0.38 M TEOA in 2.0 mL reline with 12.5% v/v water) and water (2.0 mg $^{NCN}CN_x$, 0.05 mg Pt as H_2PtCl_6, 0.38 M TEOA in 2.0 mL water pH 7) under inert conditions. After 4 h irradiation (AM 1.5G, 1 sun, 40°C, continuous N_2 purge), samples were removed from the light and centrifuged using a Sigma 1-14 Microfuge (10,000 RPM, 10 min). The supernatant was decanted and the precipitate was re-suspended in a fresh solution made up from the same solvent, but without added H_2PtCl_6 (0.38 M TEOA in 2.0 mL reline with 12.5% v/v water or 0.38 M TEOA in 2.0 mL water pH 7). The samples were purged again and irradiation was continued (AM 1.5G, 1 sun, 40°C, continuous N_2 purge).

Photocatalytic degradation of methylene blue. A conical flask open to air containing methylene blue (1 mg) and $^{NCN}CN_x$ (10 mg) in H_2O, ethaline or glyceline (100 mL) was placed in a thermostatic water bath (40°C), stirred at 600 RPM and irradiated with a solar simulator (Newport, AM 1.5G, 1 sun) for 50 min with samples (2 mL) taken every 10 min. Degradation of methylene blue was monitored by measuring the baseline-corrected absorbance at λ=668 nm.

Treatment of data. All photocatalysis, dye degradation and electrochemistry measurements were performed in triplicate and are given as the unweighted mean ± standard deviation (σ). σ of a measured value was calculated using eqn. S1. Where *n* is the number of repeated measurements, x is the value of a single measurement and $\bar{x}$ is the unweighted mean of the measurements.

$$\sigma = \sqrt{\frac{\sum(x-\bar{x})^2}{n-1}} \qquad \text{(S1)}$$

Physical Measurements

Powder X-Ray Diffraction (PXRD). PXRD was performed on a Bruker D8 X-Ray Diffractometer with Cu Kα (λ=1.54056 Å). The materials undergoing analysis were mounted and tightly packed on a zero-background spinner and diffraction patterns measured with Bragg-Brentano geometry between 10° and 80° with a step size of 0.02° for 45 minutes.

Scanning Electron Microscopy (SEM). SEM was performed on a Hitachi S4800 Scanning Electron Microscope with an electromagnetic lens. The acceleration voltage was 10 kV with a working distance of 4–400 μm. Small amounts of samples were mounted on carbon tape to ensure the samples would not be disturbed or ejected into the analysis chamber in the imaging process.

Fourier Transform Infrared Spectroscopy (FT-IR). FT-IR spectroscopy of materials was conducted with a Perkin Elmer Spectrum-Two FT-IR Spectrometer equipped with a UATR accessory.

DR-UV. UV/Vis absorption spectra were recorded on a Shimadzu UV-2550 UV-VisNIR or a Perkin Elmer Lambda 365 spectrometer using a diffuse reflectance accessory and with $BaSO_4$ as a reference material.

Sample Analysis by Gas Chromatography (GC). Gas chromatography was performed on a Shimadzu Nexis GC-2030 gas chromatograph equipped with a barrier-discharge ionisation detector (BID) and a molecular sieve column. The total run time of the method was 5 minutes. The GC was calibrated using calibration gas (2000 ppm H_2, BOC), diluted with N_2 at different ratios using a set of mass flow controllers (Bronkhorst) to provide known concentrations of H_2. Gas samples were programmed to auto-inject into the GC *via* a multi-port stream selector valve directing the selected sample purge gas stream through a 2 mL sample loop before injection. H_2 evolution rates were calculated from the measured H_2 concentration in the purge gas and the purge gas flow rate. Cumulative H_2 production was calculated from the H_2 evolution rate and time passed since the previous measurement, assuming a constant H_2 evolution rate between time points. All samples were performed in triplicate (unless otherwise stated).

Quantum efficiency (QE). Photocatalysis samples were prepared as stated above using a glass sample vial (Chromacol 10-SV, Fisher) as the photoreactor with an irradiated area A = 2.5 cm^2. Samples were purged with N_2 or air continuously during irradiation with monochromatic light (λ = 405 nm, I = 2.7 mW cm^{-2}). Hydrogen was quantified by GC using the process described above. QE was calculated according to eqn. S2.

$$\mathrm{QE}\ (\%) = \frac{2n \times N_A \times h \times c}{t_{irr} \times I \times A \times \lambda} \qquad \text{(S2)}$$

Where n is the total H_2 produced per unit time, N_A is Avogadro's Constant, h is Planck's Constant, c is the speed of light, t_{irr} is the irradiation time, I is the irradiation intensity and A is the irradiated area.

Electrochemistry. Electrochemical experiments were carried out in a thermostatic Pyrex beaker held at 40°C using an EmStat 3+ Potentiostat (PalmSens). A three-electrode setup was used with a BASi Ag/AgCl 3 M KCl (BASi) reference electrode, a 50 µm diameter Pt microwire (PtMW) working electrode and a Pt mesh counter electrode. 15.0 mL of electrolyte was used for each electrochemical experiment. All potentials are referenced versus Ag/AgCl.

Microelectrode Preparation. A PtMW electrode was fabricated according to a literature procedure (Figure S17a):[6] A rectangular window (approx. 1×3 cm) was cut out of a strip of laminating plastic foil (approx. 3×10 cm). A length of Pt microwire (50 µm diameter, Advent UK) was inserted between the laminating sheets so to expose part of the Pt wire through the window. The laminating foil was first sealed with a domestic iron, and then additionally sealed with epoxy resin to prevent the Pt wire inside the foil from coming into contact with the electrolyte.

Electrode Length Determination. The PtMW electrode length was accurately determined in a 5 mM potassium ferrocyanide solution in 0.1 M aqueous NaCl (pH not adjusted). Cyclic voltammetry (CV, v = 50 mV s^{-1}) was performed to determine the potential step parameters for chronoamperometry (Figure S17b). A potential step chronoamperogram was recorded (sampling rate 2 ms), holding at 0.0 V for 10 s before stepping to +0.6 V vs. Ag/AgCl and

holding for another 10 s (Figure S17c). A simulated current (I_{theo}) was calculated by applying the ferrocyanide concentration (5 mM) and diffusion coefficient (6.5×10^{-10} m^2 s^{-1}) to eqn. S3.[7] The fitting was optimised by a least-squares refinement of the electrode length, giving a calibrated electrode length of 3.802±0.003 cm (Figure S17c).

$$I(t) = nFlDc \times \left(\frac{\pi \times e^{-\frac{2}{5}\times\sqrt{\pi\frac{Dt}{16r^2}}}}{4\sqrt{\pi\frac{Dt}{16r^2}}} + \frac{\pi}{ln\left[\sqrt{\left(64\times e^{-0.5772\times\frac{Dt}{16r^2}}\right)+e^{\frac{5}{3}}}\right]} \right) \quad \text{(S3)}$$

Where l is the current, n is the number of transferred electrons, F is Faraday's constant, l is the electrode length, D is the O_2 diffusion coefficient, c is the O_2 concentration, t is the time, and r is the electrode radius.

O_2 Concentration Determination in DESs. The O_2 diffusion coefficient and the concentration of dissolved O_2 in the different DESs were determined by O_2 reduction at the PtMW working electrode in an analogous manner to the electrode length determination. CVs were performed in each DES (scan rate = 50 mV s^{-1}) to determine the potential step parameters E_1 and E_2 (Figure S18-S20). A potential step chronoamperogram was recorded (sampling time 2 ms) by holding at E_1 for 10 s before stepping to E_2 and holding for another 10 s. A simulated current (I_{theo}) was calculated by applying the calibrated electrode dimensions (l=2.657 cm, r=25 µm) to eqn. S3. Values for c and D were obtained by a least-squares refinement using the Origin programme, using a concatenated fit of 3 individual measurements per solvent.

Mechanistic model. The flux to the photocatalyst particle was modelled using the following variables:

- $R(hv)$: the rate of charge carrier generation at the particle surface which are available for H_2 generation.
- $R(O_2)$: the rate of O_2-induced quenching of charge carriers with concomitant consumption of O_2. Treating the photocatalyst as a spherical electrode at which O_2 reduction is diffusion limited, the rate can be described by eqn. S4 where r is the particle radius, n is the number of electrons quenched per O_2 molecule, $c(O_2)$ is the concentration of O_2 and $D(O_2)$ is the diffusion coefficient of O_2.[6]

$$R(O_2) = 4\pi \times r \times n \times D(O_2) \times c(O_2) \quad \text{(S4)}$$

- $R(H_2)$: the rate of H_2 generation. Assuming all available charges are used to generate H_2, $R(H_2)$ equals $R(hv)$, however if charge carriers are quenched by O_2, $R(H_2)$ will depend on $R(O_2)$ according to eqn. S5:

$$R(H_2) = R(hv) - R(O_2) \quad \text{(S5)}$$

- O_2 tolerance was then expressed as:

$$O_2\ tolerance = 100\% \times \frac{R(H_2)}{R(hv)} \quad \text{(S6)}$$

$$O_2\ tolerance = 100\%\ \times \frac{R(hv)-R(O_2)}{R(hv)} \quad \text{(S7)}$$

$$O_2\ tolerance = \left(1 - \frac{4\pi rn}{R(hv)} \times D(O_2) \times c(O)_2\right) \quad \text{(S8)}$$

Plotting the experimental data for $c \times D$ vs. the O_2 tolerance and performing a linear fit of all data where O_2 tolerance was >15% to eqn. S8 using the Origin programme gave:

$$\frac{4\pi rn}{R(hv)} = 3.98 \pm 0.38 \times 10^9\ \text{mol}^{-1}\ \text{m s}\ (\text{Adj. } R^2 = 0.974)$$

Supporting Figures

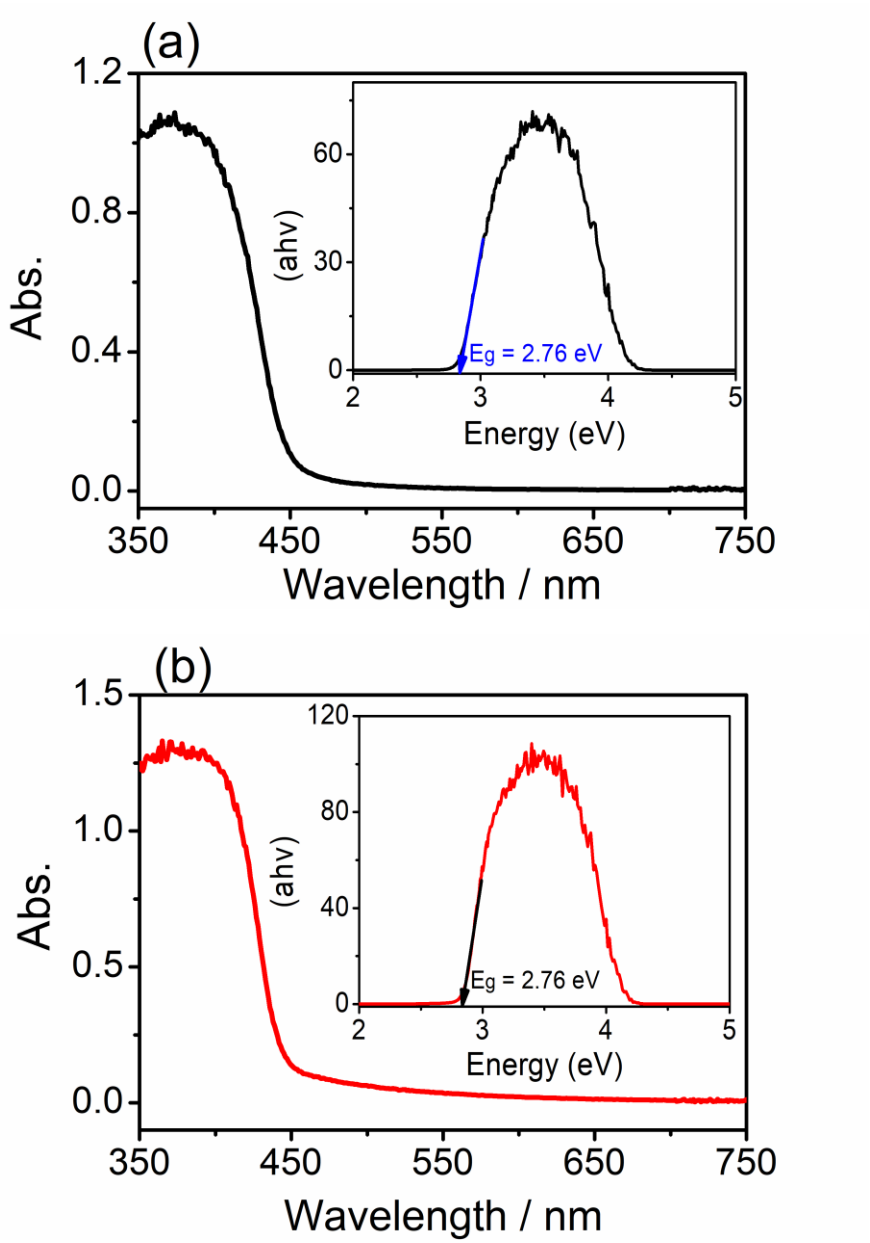

Figure S1. Absorbance spectra of (a) DCDA-CN_x and (b) $^{NCN}CN_x$. Both absorbance profiles correlate to a band gap of 2.76 eV.

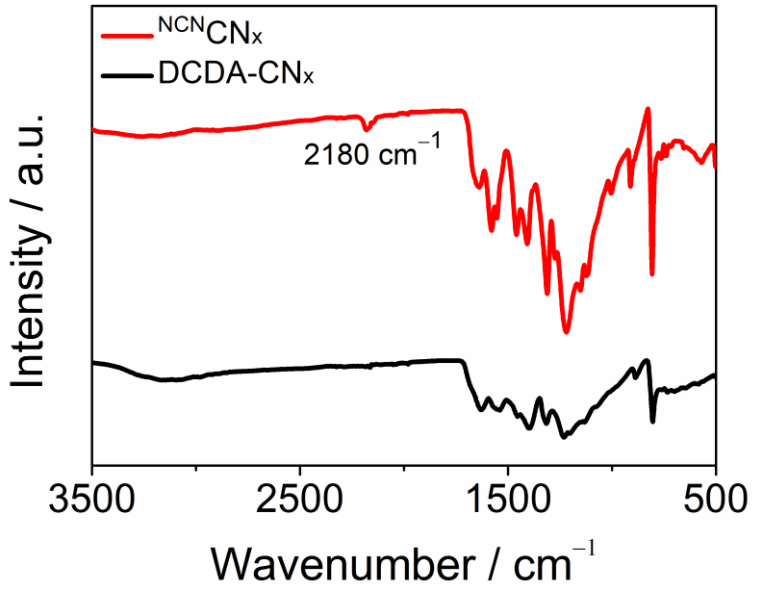

Figure S2. FT-IR Spectra of DCDA-CN_x and $^{NCN}CN_x$.

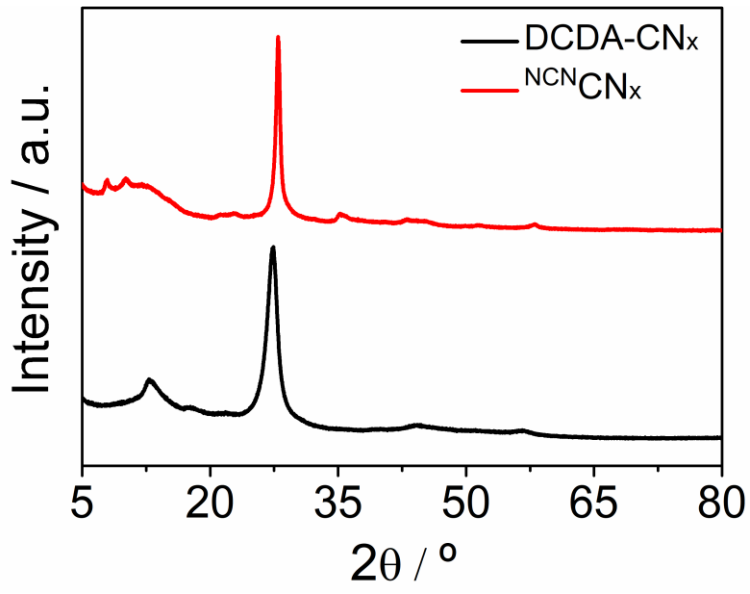

Figure S3. PXRD patterns of DCDA-CN_x and $^{NCN}CN_x$.

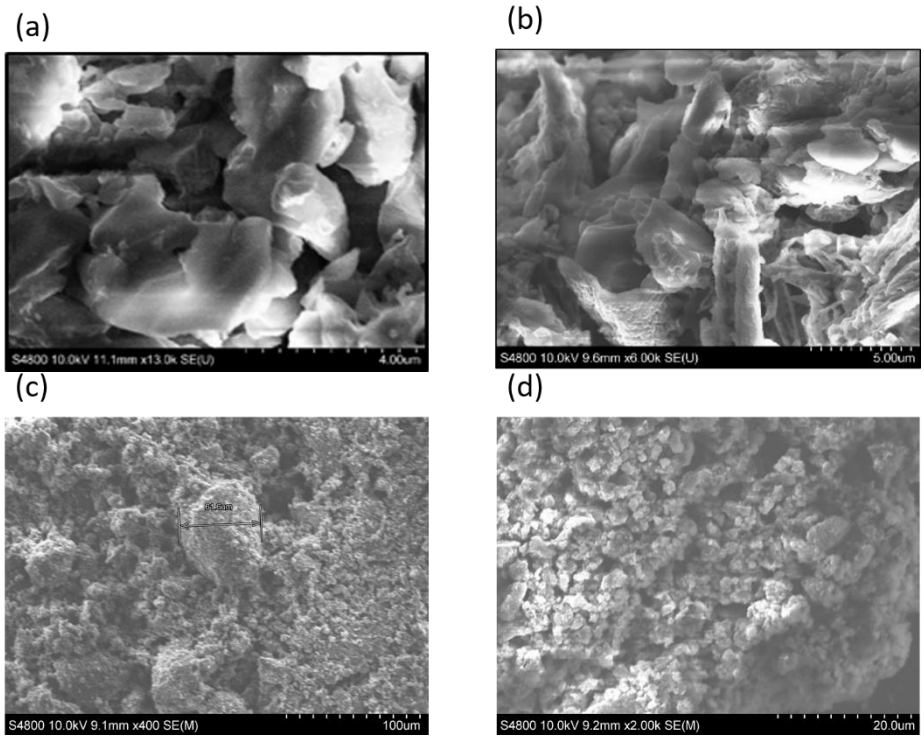

Figure S4. Scanning electron microscopy images of (a, b) DCDA-CN_x and (c, d) $^{NCN}CN_x$.

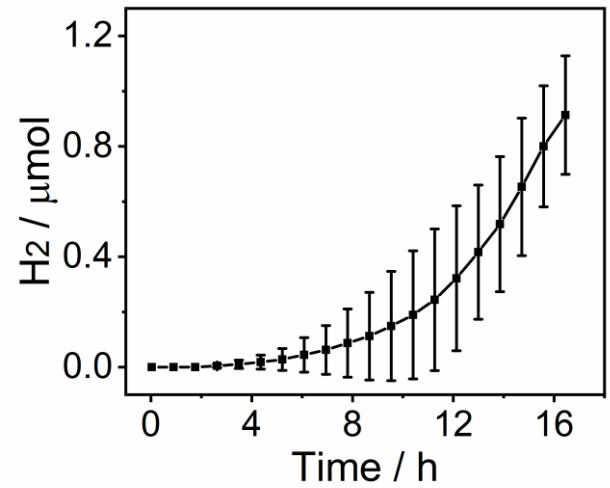

Figure S5. Cumulative photocatalytic H_2 production by $^{NCN}CN_x$ in DES solution without added H_2O. Conditions: $^{NCN}CN_x$ (2.0 mg), Pt colloids (0.05 mg), TEOA (0.38 M), MV^{2+} (2 mM) in reline (2.00 mL), AM 1.5G, 1 sun, 40°C, constant N_2 purge.

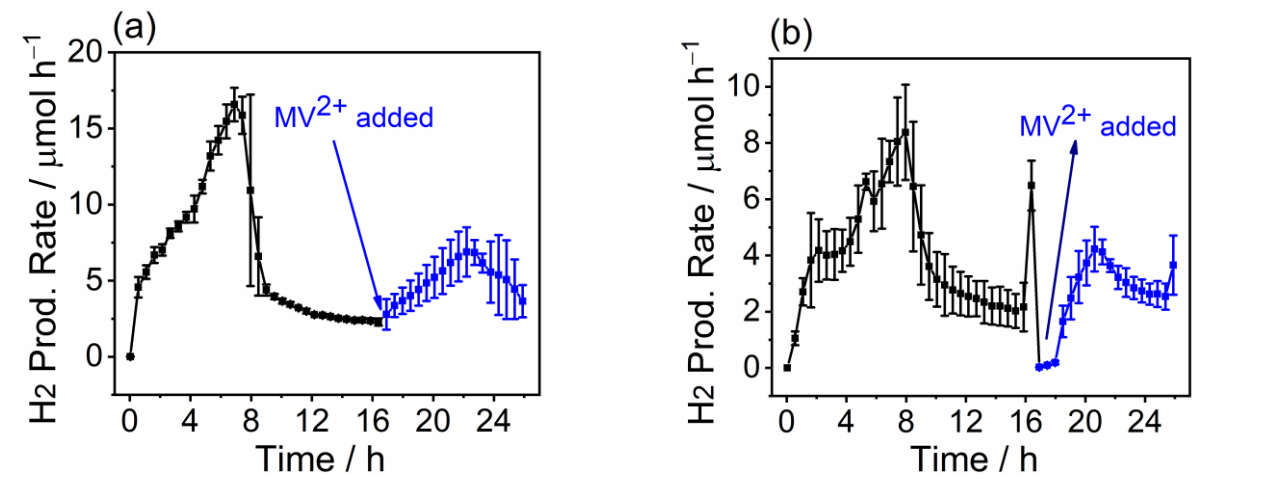

Figure S6. Effect of MV^{2+} on the photocatalytic H_2 production rate in DESs. Samples were irradiated with MV^{2+} for 17 h then further methyl viologen was added, indicated by the portion of the curve in blue. (a) in reline-based solvent, and (b) in glyceline-based solvent. Conditions: $^{NCN}CN_x$ (2.0 mg), H_2PtCl_6(0.05 mg Pt), TEOA (0.38 M), MV^{2+} (2 mM), H_2O (12.5% v/v) in (a) reline (b) glyceline (2.00 mL), AM 1.5G, 1 sun, 40°C, constant N_2 purge. A further 0.05 mL of 7.8 mM aqueous MV^{2+} solution was added after 17 h.

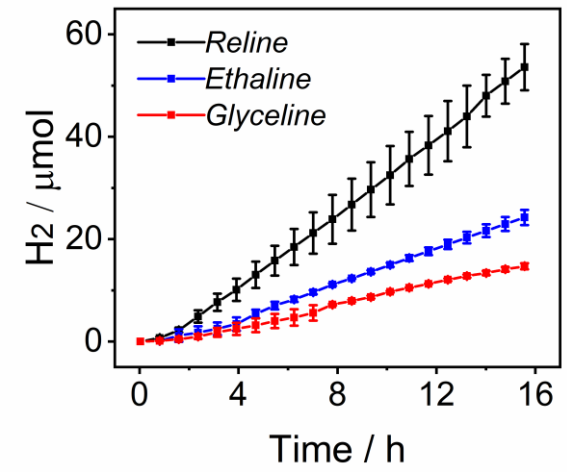

Figure S7. Photocatalytic H_2 generation in DESs at Pt/^{NCN}CN in the absence of a redox mediator. Conditions: $^{NCN}CN_x$ (2.0 mg), H_2PtCl_6(0.05 mg Pt) in 2.00 mL DES (12.5% H_2O, 0.38 M TEOA), AM 1.5G, 1 sun, 40°C, constant N_2 purge.

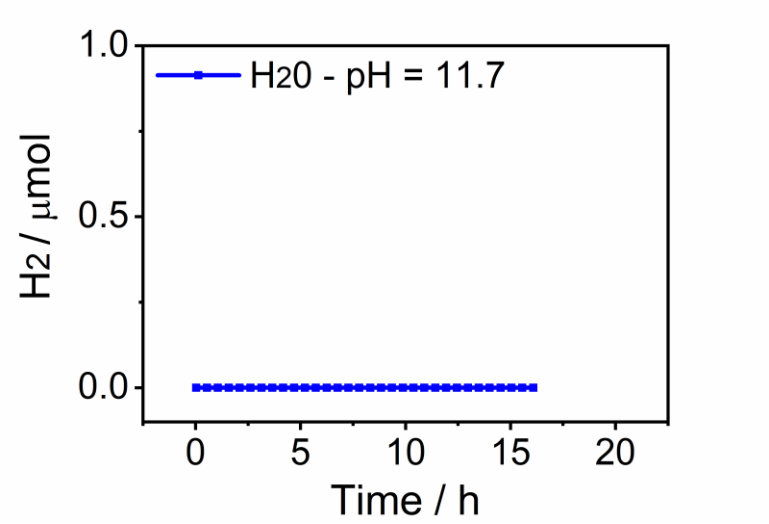

Figure S8. Photocatalytic H_2 production at $^{NCN}CN_x$ in aqueous TEOA solution without pH adjustment (pH 11.7). Conditions: $^{NCN}CN_x$ (2.0 mg), H_2PtCl_6 (0.05 mg Pt), TEOA (0.38 M), MV^{2+} (2 mM) in H_2O (2.00 mL), AM 1.5G, 1 sun, 40°C, constant N_2 purge.

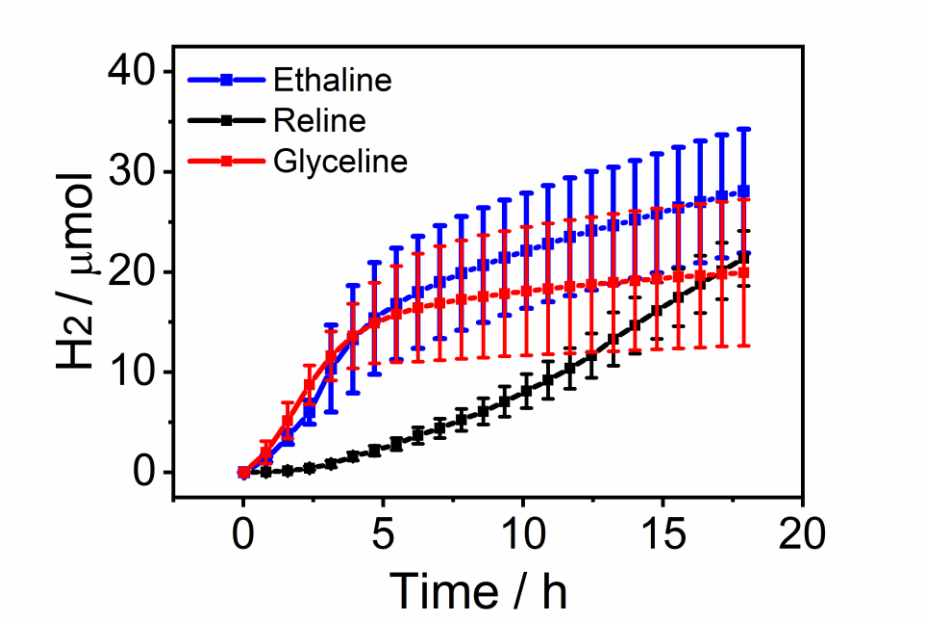

Figure S9. Photocatalytic H_2 production by $^{NCN}CN_x$ in DESs in the absence of TEOA. Conditions: $^{NCN}CN_x$ (2.0 mg), H_2PtCl_6 (0.05 mg Pt), MV^{2+} (2 mM), H_2O (12.5% v/v) in ethaline, reline or glyceline (2.00 mL), AM 1.5G, 1 sun, 40°C, constant N_2 purge.

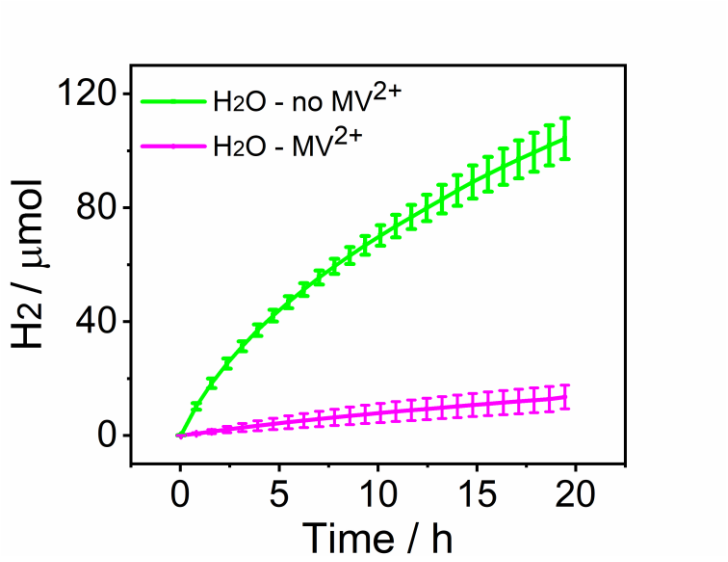

Figure S10. Photocatalytic H_2 generation at Pt/$^{NCN}CN_x$ in water. Conditions: $^{NCN}CN_x$ (2.0 mg), H_2PtCl_6 (0.05 mg Pt) in 2.00 mL water (0.38 M TEOA, pH 7); with or without MV^{2+} (2 mM); AM 1.5G, 1 sun, 40°C, constant N_2 purge.

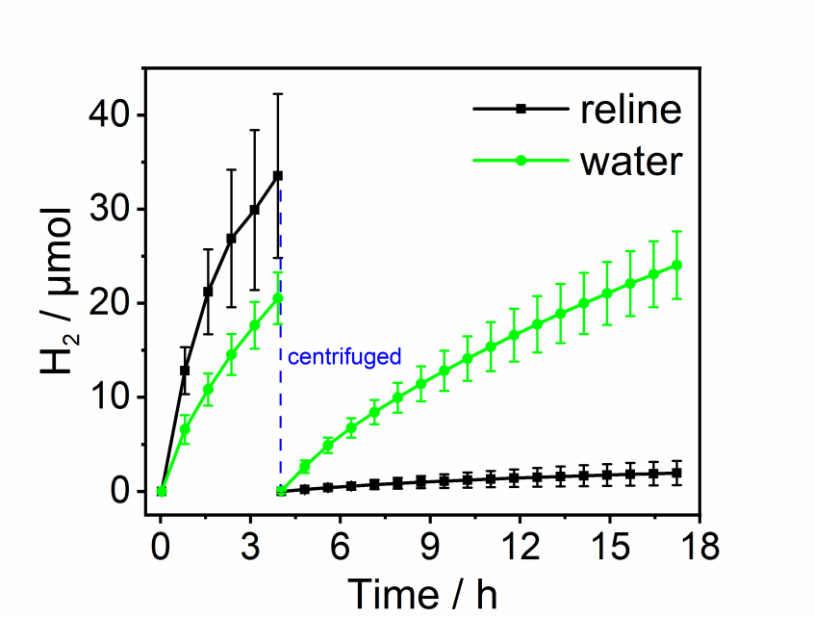

Figure S11. Study of the influence of the solvent on co-catalyst attachment. Photocatalytic H_2 generation at Pt/$^{NCN}CN_x$ was performed under standard conditions for in water and reline (2.0 mg $^{NCN}CN_x$, 0.05 mg Pt as H_2PtCl_6, 0.38 M TEOA) in 2.00 mL water pH 7 or reline with 12.5% v/v water; AM 1.5G, 1 sun, 40°C, continuous N_2 purge). After 4 h irradiation, samples were centrifuged, and the separated precipitate was re-suspended in fresh solution (0.38 M TEOA in 2.0 mL water pH 7 or reline with 12.5% v/v water) without added H_2PtCl_6 before irradiation was continued (AM 1.5G, 1 sun, 40°C, constant N_2 purge).

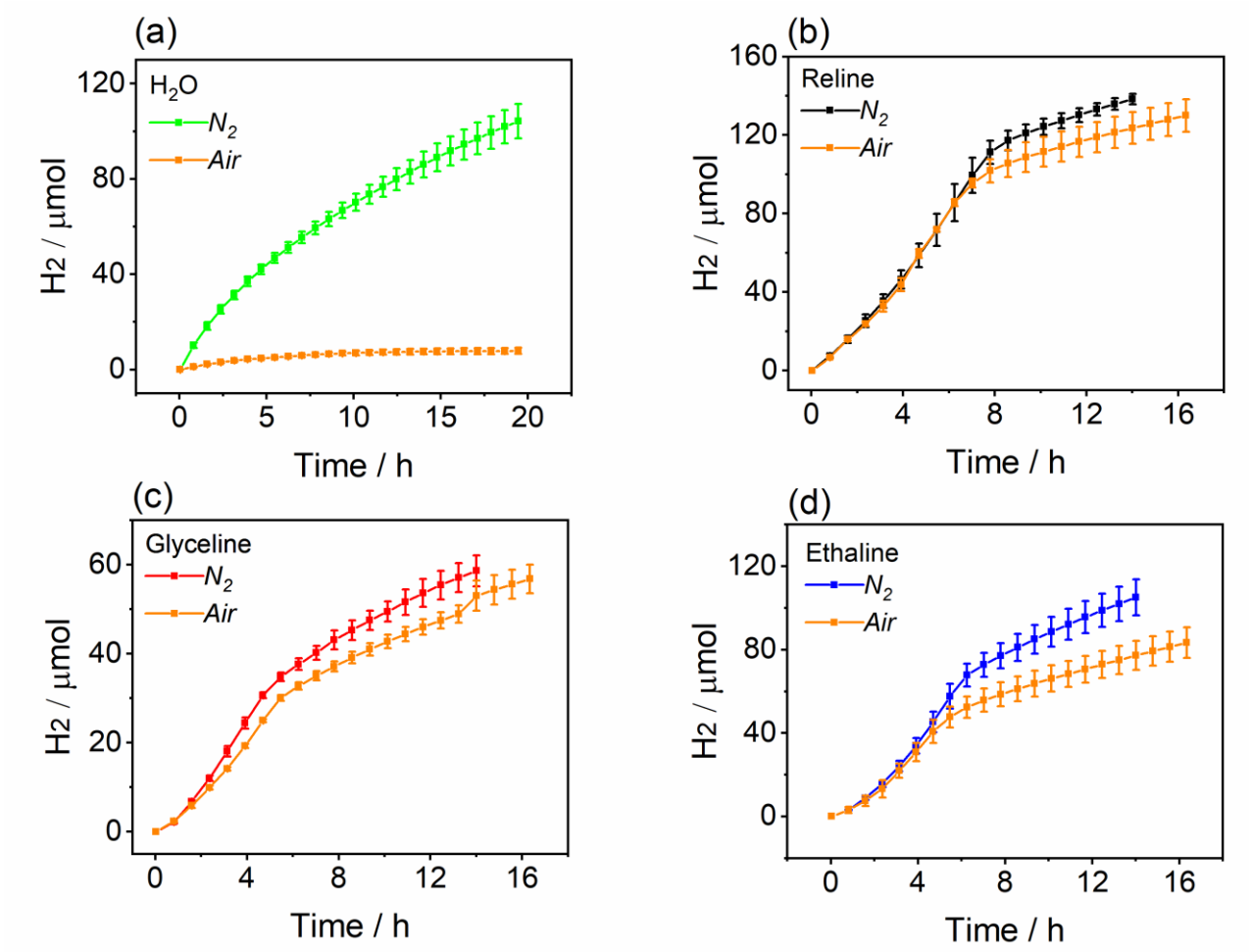

Figure S12. Effect of aerobic conditions on H_2 production in H_2O (a) reline, (b) glyceline (c) and ethaline (d). Conditions: $^{NCN}CN_x$ (2.0 mg), H_2PtCl_6 (0.05 mg Pt) in 2.00 mL DES (12.5% H_2O, 0.38 M TEOA, 2 mM MV^{2+}) or water (0.38 M TEOA, pH 7); AM 1.5G, 1 sun, 40°C, constant air purge.

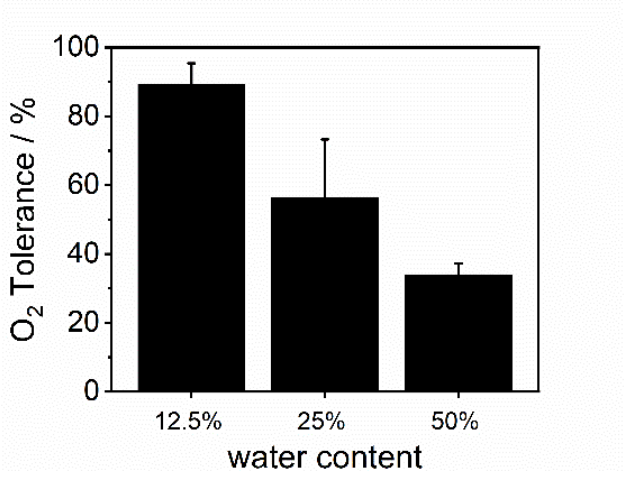

Figure S13. Photocatalytic H_2 generation at Pt/$^{NCN}CN_x$ in the presence of varying amounts of added water. Conditions: $^{NCN}CN_x$ (2.0 mg), H_2PtCl_6 (0.05 mg Pt) 0.38 M TEOA, 2 mM MV^{2+} in reline/water mixtures (2.00 mL; 12.5, 25 or 50% v/v H_2O); AM 1.5G, 1 sun, 40°C). Constant N_2 or air purge, 14 h irradiation.

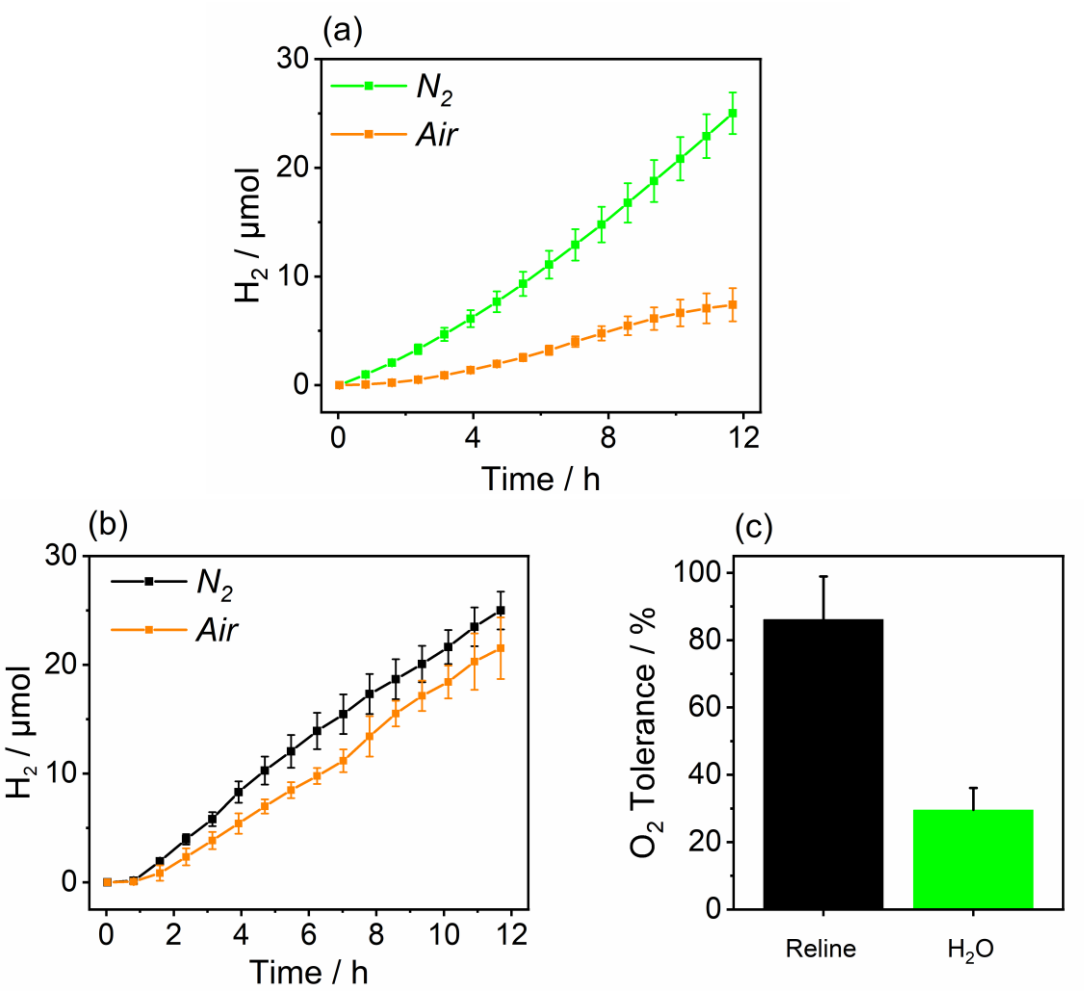

Figure S14. Photocatalytic H_2 generation by Pt/TiO_2 in different solvents. (a) H_2 generation by Pt/TiO_2 in water and (b) in reline. (c) O_2 tolerance of the H_2 generation by Pt/TiO_2 depending on the solvent after 11.7 h. Conditions: TiO_2 P25 (2 mg), H_2PtCl_6 (0.05 mg Pt), MV^{2+} (2 mM), 0.38 M TEOA in H_2O (2.0 mL, pH 7) or reline (12.5% v/v H_2O, 2.00 mL). Constant N_2 or air purge.

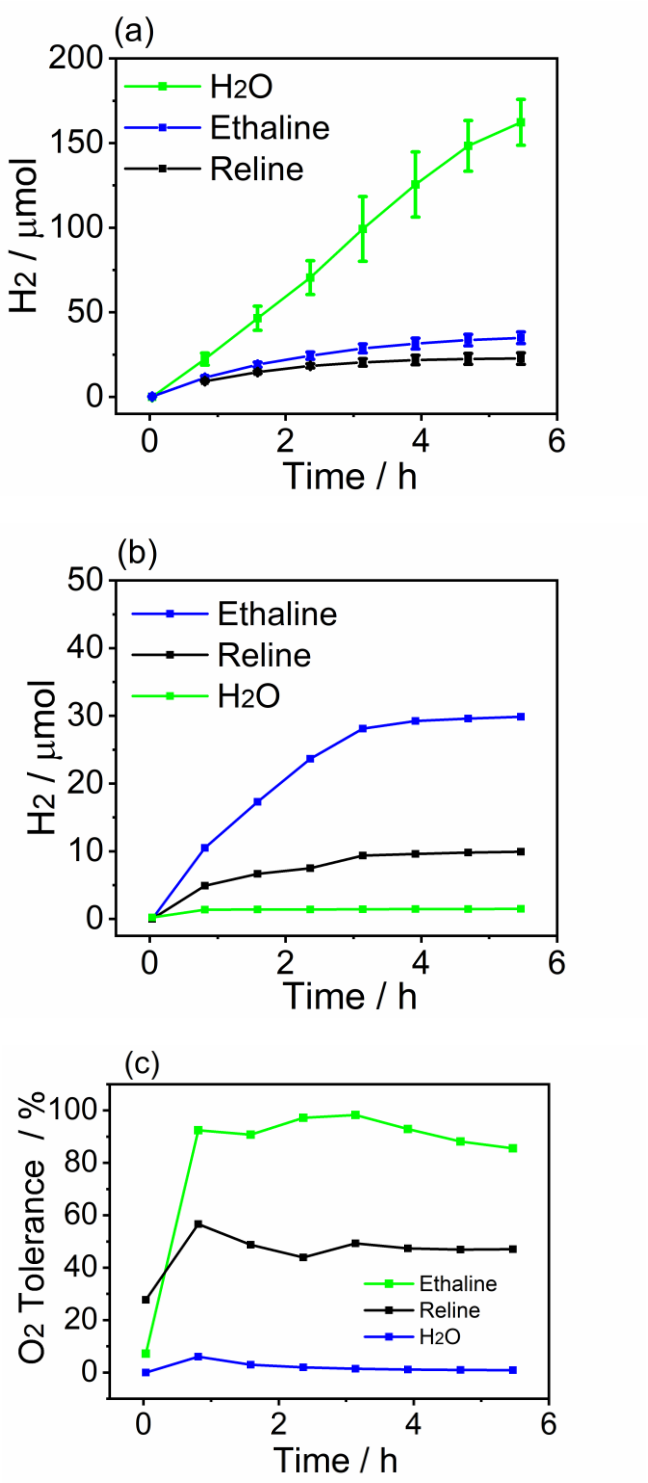

Figure S15. Photocatalytic H_2 generation by Pt/Eosin Y in different solvents. (a) H_2 generation by Pt/Eosin Y in anaerobic environment. (b) H_2 generation by Pt/Eosin Y in the presence of air. Reactions performed in singlets. (c) O_2 tolerance of the H_2 generation by Pt/Eosin Y. Conditions: Eosin Y (2 mM), Pt colloids (0.05 mg), MV^{2+} (2 mM), 0.38 M TEOA in H_2O (2.00 mL, pH 7) or DES (12.5% v/v water in 2.00 mL ethaline or reline). Constant N_2 or air purge.

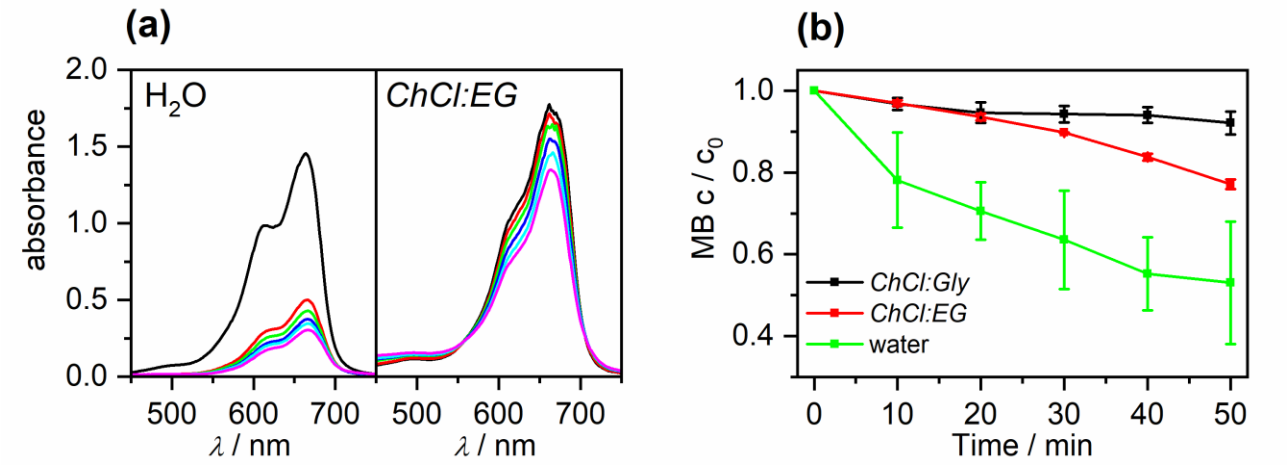

Figure S16. (a) Photocatalytic degradation of methylene blue (MB) at $^{NCN}CN_x$ in H_2O and ethaline, spectra taken every 10 min; (b) Photocatalytic degradation of MB in different solvents over time. Conditions: MB (10 mg L^{-1}), $^{NCN}CN_x$ (100 mg L^{-1}) in DES or water (100 mL); AM 1.5G, 1 sun, 40°C, open to air).

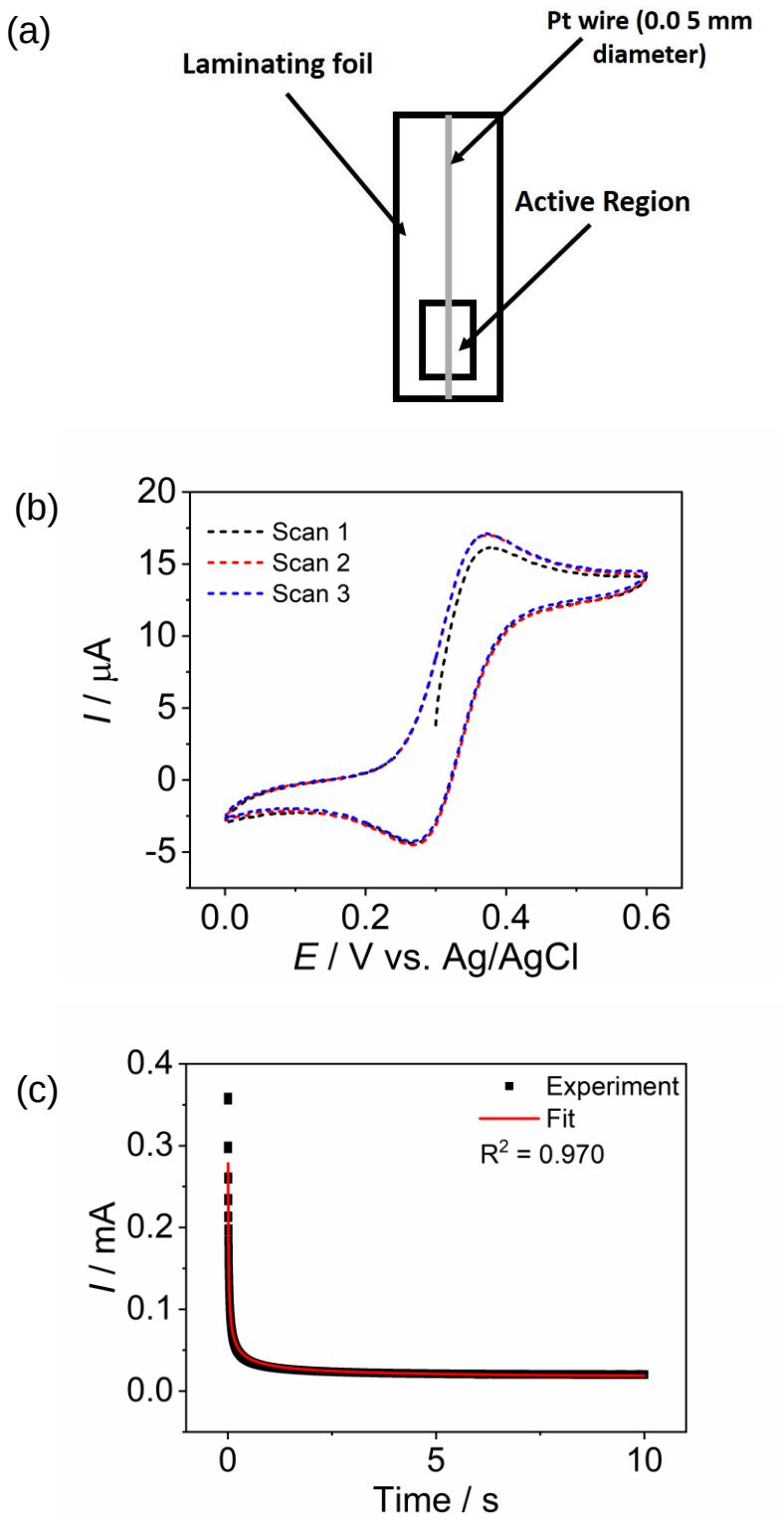

Figure S17. Pt microwire electrochemistry. (a) Schematic representation of a Pt microwire electrode. (b) Cyclic voltammogram (scan rate = 50 mV s^{-1}) of 5 mM potassium ferrocyanide in 1 M NaCl solution using a Pt microwire working electrode. (c) Chronoamperometric response of a Pt microwire working electrode in 5 mM ferrocyanide solution to a potential step from 0.0 V to +0.6 V vs. Ag/AgCl. Chronoamperogram was fitted according to eqn. S3 to determine the calibrated electrode length to be *l* = 3.802±0.003 cm.

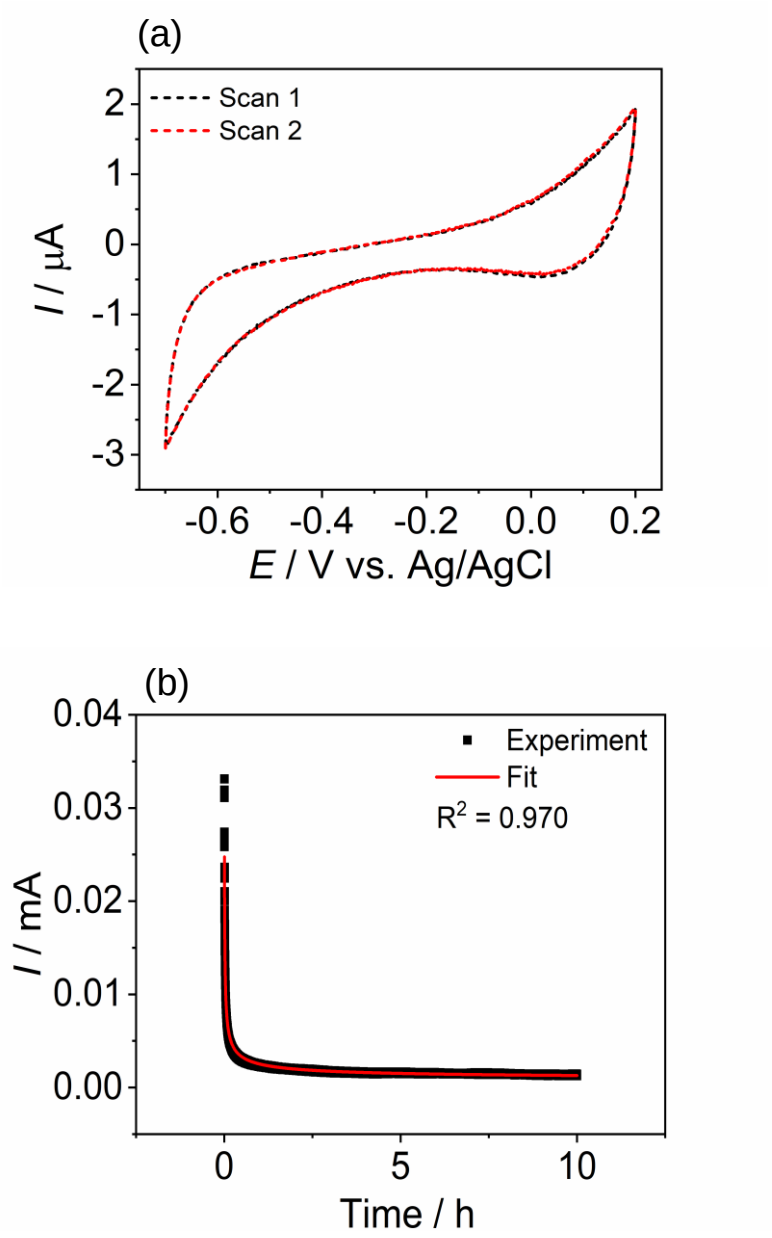

Figure S18. Determination of O_2 solubility and diffusivity in reline. (a) Cyclic voltammogram of reline-H_2O-TEOA (82.5%:12.5%:5% v/v) at 40 °C (v = 50 mV s^{-1}). (b) Superposition of 3 O_2 reduction chronoamperograms (2 ms sampling rate, total run time 10 s) upon stepping from 0.2 V to −0.7 V vs. Ag/AgCl and the concatenated fit according to eqn. S3 using $D(O_2)=2.93\times10^{-10}$ m^2 s^{-1} and $c(O_2)$=167.8 µM (first two data points of each chronoamperogram were excluded from the fit).

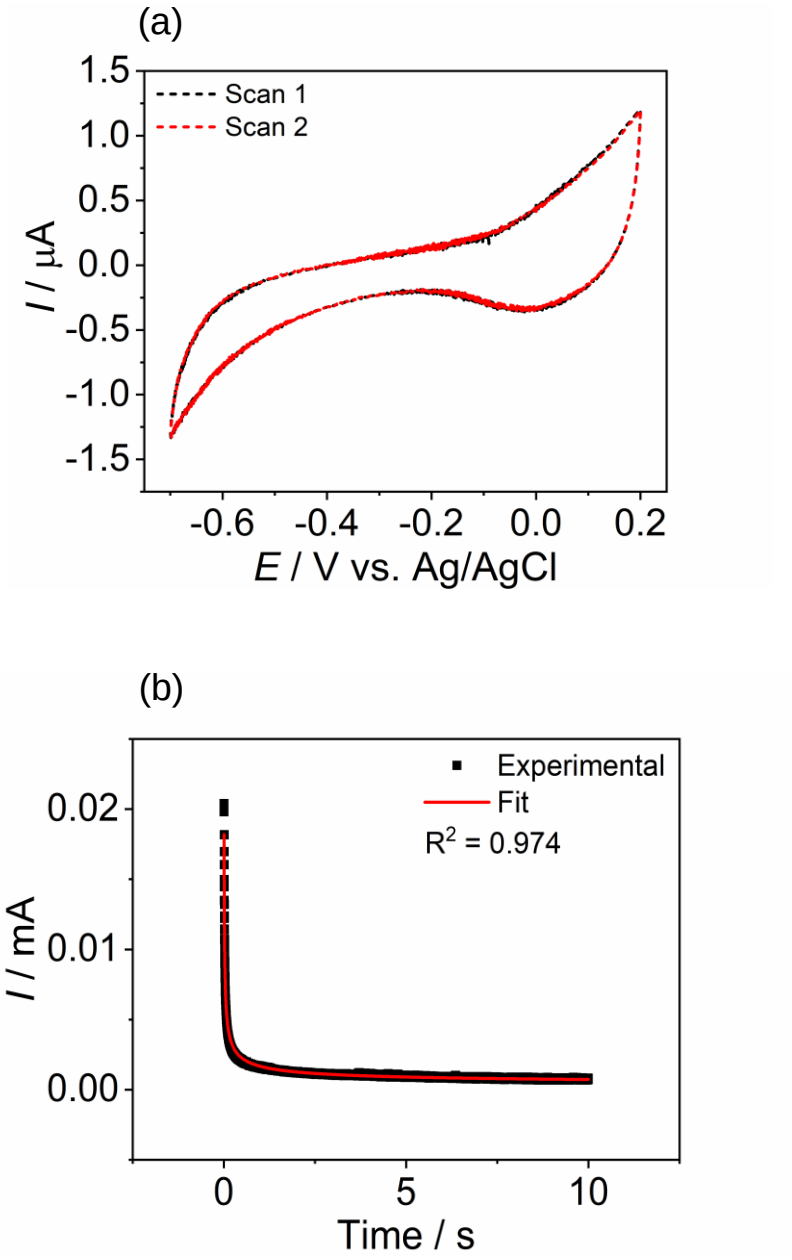

Figure S19. Determination of O_2 solubility and diffusivity in glyceline. (a) Cyclic voltammogram of glyceline-H_2O-TEOA at 40°C (v = 50 mV s^{-1}). (b) Superposition of 3 O_2 reduction chronoamperograms (2 ms sampling rate, total run time 10 s) upon stepping from 0.2 V to −0.7 V vs. Ag/AgCl and the concatenated fit according to eqn. S3 using $D(O_2)=9.52\times10^{-11}$ m^2 s^{-1} and $c(O_2)=218.8$ µM (first two data points of each chronoamperogram were excluded from the fit).

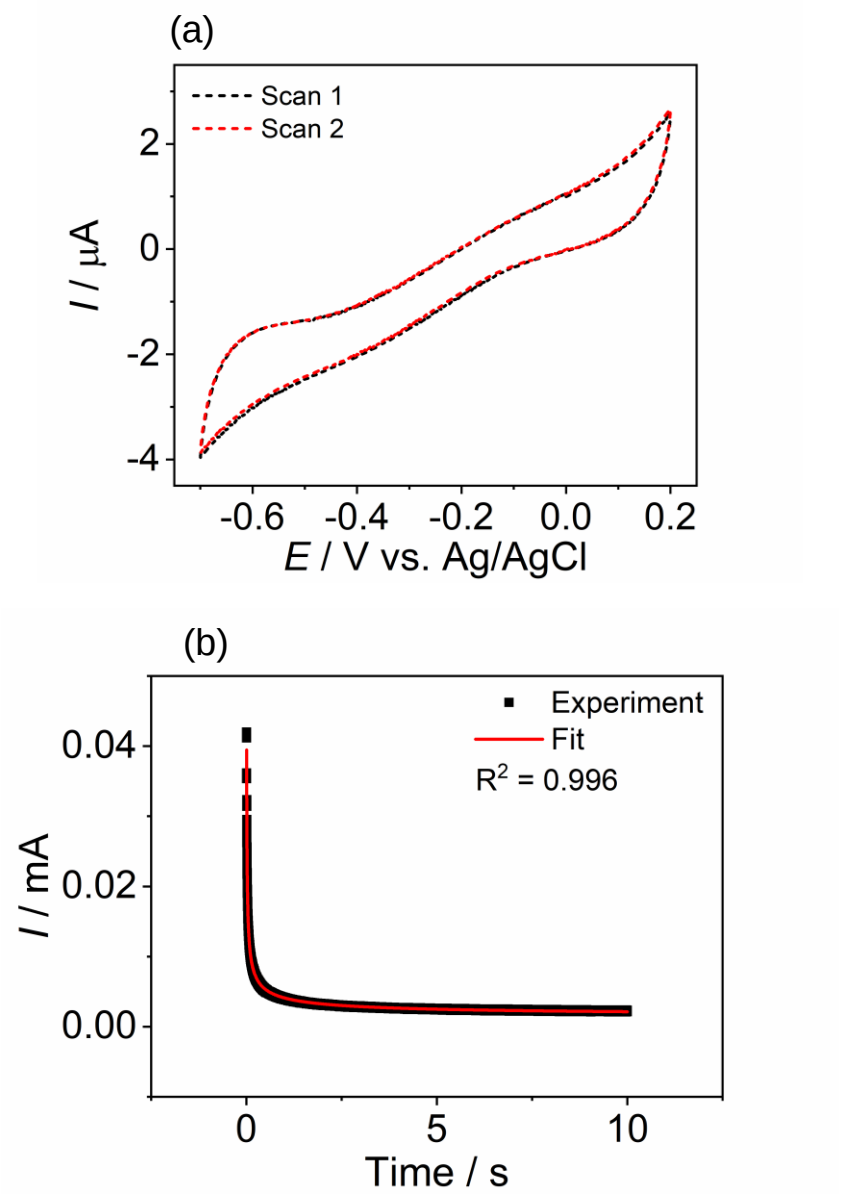

Figure S20. Determination of O_2 solubility and diffusivity in ethaline-H_2O-TEOA at 40 °C. (a) Cyclic voltammogram of aerated ethaline-H_2O-TEOA at 40 °C. (v = 50 mV s^{-1}). (b) Superposition of 3 O_2 reduction chronoamperograms (2 ms sampling rate, total run time 10 s) upon stepping from 0.2 V to −0.9 V vs. Ag/AgCl and the concatenated fit according to eqn. S3 using $D(O_2)=3.32\times10^{-10}$ m^2 s^{-1} and $c(O_2)$=250.7 µM (first two data points of each chronoamperogram were excluded from the fit).

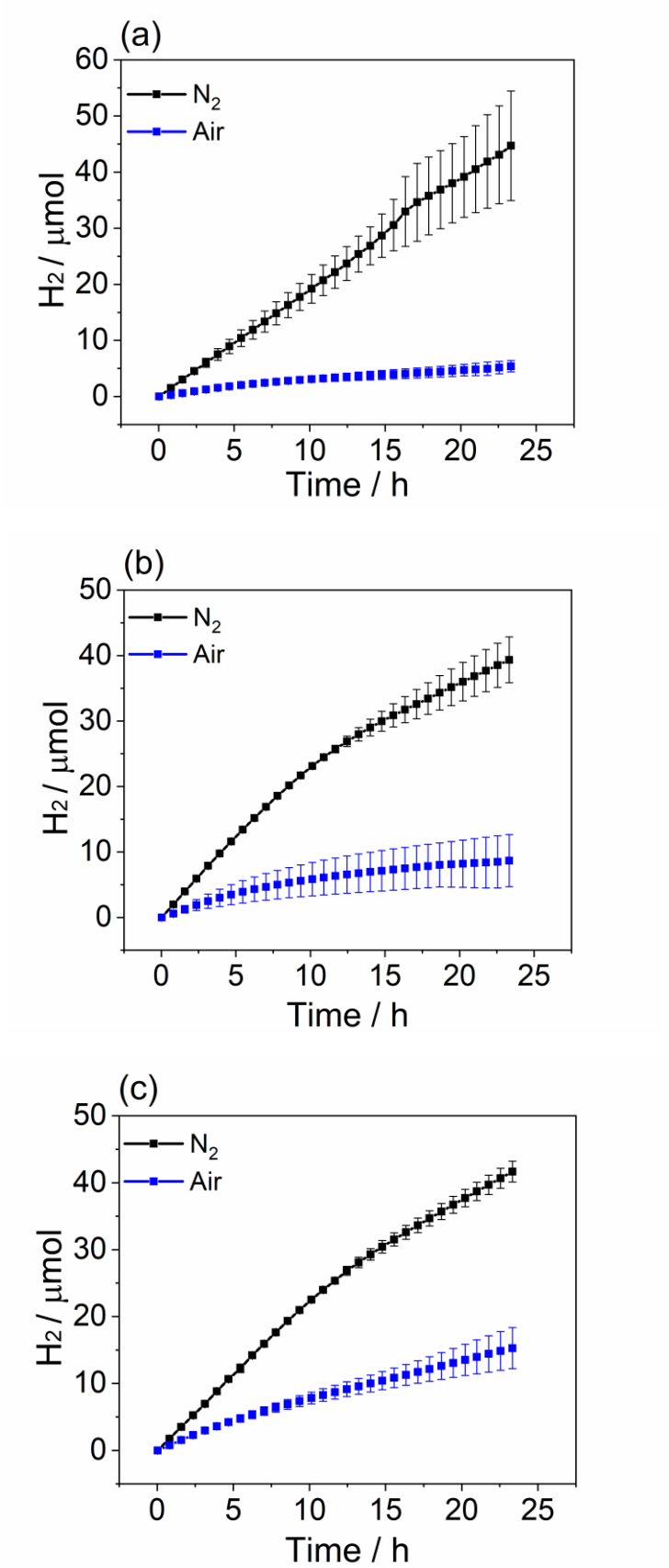

Figure S21. Photocatalytic H_2 production in brine solutions of varying concentrations examined under inert and aerobic atmospheres, (a) 1 M NaCl (b) 2 M NaCl and (c) 4 M NaCl. Conditions: $^{NCN}CN_x$ (2.0 mg), H_2PtCl_6 (0.05 mg Pt), TEOA (0.38 M), methyl viologen (2 mM), NaCl (1, 2 or 4 M), in H_2O (2.00 mL, pH 7.0), AM 1.5G, 1 sun, 40°C, constant N_2 or air purge.

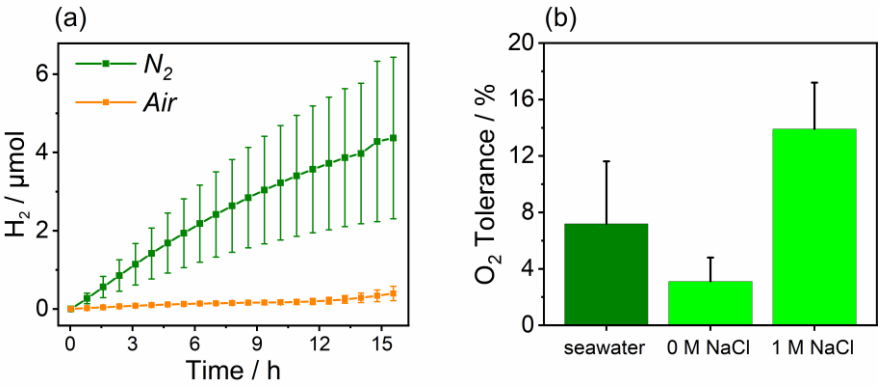

Figure S22. Photocatalytic H_2 generation at Pt/$^{NCN}CN_x$ using seawater as the solvent. (a) H_2 production in anaerobic and aerobic conditions. (b) O_2 tolerance after 14 h irradiation in different solvents. Conditions: $^{NCN}CN_x$ (2.0 mg), H_2PtCl_6 (0.05 mg Pt), 0.38 M TEOA, 2 mM MV^{2+} in 2.00 mL seawater (collected from Swansea Beach), water or 1 M NaCl, pH adjusted to 7.0; AM 1.5G, 1 sun, 40°C. Constant N_2 or air purge.

Supporting Tables

Table S1. Photocatalytic H_2 generation in DES-based solutions in inert conditions (AM 1.5G, 1 sun, 40 °C, purge gas at 4 mL min^{-1}).

Solvent		H_2O	$^{NCN}CN_x$	H_2PtCl_6	TEOA	pH[a]	MV^{2+}	Purge Gas	Max. H_2 rate	Activity	total H_2 [b]
	mL	mL	mg	mg Pt	M		mM		μmol h^{-1}	mmol $h^{-1}g^{-1}_{cat}$	μmol
reline	1.75	0.25	2.0	0.05	0.38	n. a.	2.0	N_2	17.9±1.7	8.9±0.9	138.3±2.6
ethaline	1.75	0.25	2.0	0.05	0.38	n. a.	2.0	N_2	15.9±1.4	8.0±0.7	105.1±8.6
glyceline	1.75	0.25	2.0	0.05	0.38	n. a.	2.0	N_2	8.2±0.2	4.1±0.1	58.7±3.5
water		2.00	2.0	0.05	0.38	7.0	2.0	N_2	0.96±0.54	0.48±0.27	10.2±4.0
reline	1.75	0.25	2.0	0.05	0.38	n. a.	0	N_2	4.7±2.5	2.4±1.3	43.2±3.7
ethaline	1.75	0.25	2.0	0.05	0.38	n. a.	0	N_2	2.5±1.3	1.3±0.7	21.6±1.3
glyceline	1.75	0.25	2.0	0.05	0.38	n. a.	0	N_2	2.1±1.8	1.1±0.9	13.4±0.4
water		2.00	2.0	0.05	0.38	7.0	0	N_2	13.0±1.4	6.5±0.7	86.1±5.4

[a] n.a. = not adjusted; [b] after 14.0 h irradiation

Table S2. External quantum efficiency (QE) determination for anaerobic photocatalytic H_2 evolution with 2.0 mg Pt/CN_x in 2.0 mL reline-H_2O-TEOA (82.5%:12.5%:5% v/v); I = 2.69 mW cm^{-2}, A = 2.5 cm^2, λ = 405 nm, 40 °C, constant N_2 purge at 4 mL min^{-1}.

Time	n(H_2)	QE
h	μmol	%
1	1.7±0.7	3.9±1.6
2	2.4±1.0	2.9±1.1
3	3.2±1.1	2.5±0.8
4	4.2±1.5	2.6±0.9
5	5.4±1.2	2.6±0.6
10	13.1±4.7	3.1±1.19
15	21.7±9.3	3.5±1.5
20	30.8±12.6	3.7±1.5

Table S3. Photocatalytic H_2 generation in DES-based solutions in aerobic conditions (AM 1.5G, 1 sun, 40 °C, purge gas at 4 mL min^{-1}).

Solvent		H_2O	$^{NCN}CN_x$	H_2PtCl_6	TEOA	pH[a]	MV^{2+}	Purge Gas	Max. H_2 rate	Activity	total H_2 [b]	O_2 Tolerance[c]
	mL	mL	mg	mg Pt	M		mM		µmol h^{-1}	mmol $h^{-1}g^{-1}_{cat}$	µmol	%
reline	1.75	0.25	2.0	0.05	0.38	n. a.	2.0	Air	20.4±7.1	10.2±3.6	123.5±8.1	89.3±7.5
ethaline	1.75	0.25	2.0	0.05	0.38	n. a.	2.0	Air	12.7±1.5	6.4±0.8	77.3±6.9	73.7±12.9
glyceline	1.75	0.25	2.0	0.05	0.38	n. a.	2.0	Air	7.3±0.3	3.7±0.2	53.0±3.3	90.4±11.1
water		2.00	2.0	0.05	0.38	7.0	0	Air	1.5±0.3	0.75±0.15	7.6±1.2	8.8±1.5
water		2.00	2.0	0.05	0.38	7.0	2.0	Air	0.1±0.08	0.05±0.04	0.3±0.1	2.4±0.1

[a] n.a. = not adjusted; [b] after 15.5 h irradiation; [c] O_2 tolerance = n(H_2) produced under air relative to n(H_2) produced under N_2 after 14.0 h irradiation.

Table S4. External quantum efficiency (QE) determination for photocatalytic H_2 evolution with 2.0 mg Pt/CN_x in 2.0 mL reline-H_2O-TEOA (82.5%:12/5%:5% v/v); I = 2.70 mW cm^{-2}, A = 2.5 cm^2, λ = 405 nm, 40 °C, constant air purge at 4 mL min^{-1}.

Time	n(H_2)	QE
h	µmol	%
1	1.4±0.6	3.2±1.5
2	2.0±0.6	2.3±0.7
3	3.0±1.0	2.3±0.8
4	3.9±1.1	2.4±0.7
5	5.3±1.0	2.6±0.5
10	14.7±2.0	3.5±0.5
15	23.4±2.6	3.8±0.4
20	32.2±2.9	3.9±0.3

Table S5. Literature examples of O_2-tolerant H_2 evolution.

Photocatalyst	O_2 Tolerance	Flow Type	Reference
Ni_2P/CdS	46.1%	Closed chamber	[8]
MoS_2/CdS	61.9%	Closed chamber	[9]
CoP/CdS	79.8%	Closed chamber	[10]
WS_2-MoS_2/CdS	65.1%	Closed chamber	[11]
CdS	30.5%	Sealed chamber	[12]
CdS/CoO_x	>100%	Continuous purge	[13]
PFBT Pdots	37%	Closed chamber	[14]
Ni_2P/OH-GQDs	64%	Closed chamber	[15]
RuP/CoP/TiO_2	17%	Closed chamber	[16]
CoP/EY	70±4%	Closed chamber	[16]
[SO_3 Ph_2phenRu_2]Rh	60%	Closed chamber	[17]
[Ru(dnbpy)(tbbpy)$_2$](PF_6)$_2$ / [Co(dmgH)$_2$]	n/a	Closed chamber O_2 reduction *in situ*	[18]
Ru(mmip)[PF_6]$_3$/ Co(dmgH)$_2$	n/a	Closed chamber O_2 reduction *in situ*	[19]
[Ru(bpy$_3$)]$^{2+}$/[Co(DPA-Bpy)(H_2O)](PF_6)$_3$	40%	Closed chamber	[20]
[Ir(ppy)$_2$(bpy)]PF_6 / [Co(CF_3SO_3)(Py_2^{Ts}tacn)][CF_3SO_3]	25%	Closed chamber	[21]
Ru(bpy)$_3^{2+}$ / MV^{2+} / PGP50-H_2ase	71.8%	Closed chamber	[22]
[Ru(bpy)$_2$(NH_2phen)](PF_6)$_2$ – H_2ase	11.1%	Closed chamber	[23]
Db [NiFeSe] hydrogenase / EY	10%	Closed chamber	[24]
Pt/$^{NCN}CN_x$	99% from max rate 89.4±13.7% from total H_2 after 15 h	Continuous purge	this work
Pt/Eosin Y	94% from max rate 85% from total H_2 after 6 h	Continuous Purge	this work

Table S6. Photocatalytic H_2 generation in brines (AM 1.5G, 1 sun, 40 °C, purge gas at 4 mL min^{-1}).

Solvent		$^{NCN}CN_x$	H_2PtCl_6	TEOA	pH[a]	MV^{2+}	Purge Gas	Max. H_2 rate	total H_2 [b]
	mL	mg	mg Pt	M		mM		µmol h^{-1}	µmol
water	2.00	2.0	0.05	0.38	7.0	2.0	N_2	0.60±0.2	10.2±4.0
1 M NaCl	2.00	2.0	0.05	0.38	7.0	2.0	N_2	1.9±0.3	28.9±3.4
2 M NaCl	2.00	2.0	0.05	0.38	7.0	2.0	N_2	1.3±0.4	29.0±1.3
4 M NaCl	2.00	2.0	0.05	0.38	7.0	2.0	N_2	1.5±0.1	29.3±0.9
water	2.00	2.0	0.05	0.38	7.0	2.0	Air	0.1±0.08	0.3±0.1
1 M NaCl	2.00	2.0	0.05	0.38	7.0	2.0	Air	0.1±0.1	3.7±0.8
2 M NaCl	2.00	2.0	0.05	0.38	7.0	2.0	Air	0.3±0.1	5.5±3.3
4 M NaCl	2.00	2.0	0.05	0.38	7.0	2.0	Air	0.5±0.1	10.2±1.5

[a] adjusted with 1 M HCl; [b] after 15.5 h irradiation.

Supporting references

1. S. Cao, J. Low, J. Yu and M. Jaroniec, *Adv. Mater.*, 2015, **27**, 2150-2176.
2. V. W.-h. Lau, I. Moudrakovski, T. Botari, S. Weinberger, M. B. Mesch, V. Duppel, J. Senker, V. Blum and B. V. Lotsch, *Nat. Commun.*, 2016, **7**, 12165.
3. F. Fina, S. K. Callear, G. M. Carins and J. T. S. Irvine, *Chem. Mater.*, 2015, **27**, 2612-2618.
4. A. P. Abbott, D. Boothby, G. Capper, D. L. Davies and R. K. Rasheed, *J. Am. Chem. Soc.*, 2004, **126**, 9142-9147.
5. A. P. Abbott, G. Capper, D. L. Davies, R. K. Rasheed and V. Tambyrajah, *Chem. Commun.*, 2003, 70-71.
6. J. Weber, A. J. Wain and F. Marken, *Electroanalysis*, 2015, **27**, 1829-1835.
7. A. Neudeck and L. Kress, *J. Electroanal.l Chem.*, 1997, **437**, 141-156.
8. Z. Sun, H. Zheng, J. Li and P. Du, *Energy Environ. Sci.*, 2015, **8**, 2668-2676.
9. D. A. Reddy, H. Park, S. Hong, D. P. Kumar and T. K. Kim, *J. Mater. Chem. A*, 2017, **5**, 6981-6991.
10. S. Cao, Y. Chen, C.-J. Wang, X.-J. Lv and W.-F. Fu, *Chem. Commun.*, 2015, **51**, 8708-8711.
11. D. A. Reddy, H. Park, R. Ma, D. P. Kumar, M. Lim and T. K. Kim, *ChemSusChem*, 2017, **10**, 1563-1570.
12. L. Ma, M. Liu, D. Jing and L. Guo, *J Mater. Chem. A*, 2015, **3**, 5701-5707.
13. D. W. Wakerley, K. H. Ly, N. Kornienko, K. L. Orchard, M. F. Kuehnel and E. Reisner, *Chem. Eur. J.*, 2018, **24**, 18385-18388.
14. L. Wang, R. Fernández-Terán, L. Zhang, D. L. A. Fernandes, L. Tian, H. Chen and H. Tian, *Angew. Chem. Int. Ed.*, 2016, **55**, 12306-12310.
15. L. Zhu, Q. Yue, D. Jiang, H. Chen, R. Muhammad Irfan and P. Du, *Chinese J. Catal.*, 2018, **39**, 1753-1761.
16. F. Lakadamyali, M. Kato, N. M. Muresan and E. Reisner, *Angew. Chem. Int. Ed.*, 2012, **51**, 9381-9384.
17. T. R. Canterbury, S. M. Arachchige, K. J. Brewer and R. B. Moore, *Chem. Commun.*, 2016, **52**, 8663-8666.
18. R. Staehle, S. Losse, M. R. Filipovic, I. Ivanović-Burmazović, J. G. Vos and S. Rau, *ChemPlusChem*, 2014, **79**, 1614-1621.
19. L. Petermann, R. Staehle, M. Pfeifer, C. Reichardt, D. Sorsche, M. Wächtler, J. Popp, B. Dietzek and S. Rau, *Chem. Eur. J.,* 2016, **22**, 8240-8253.
20. W. M. Singh, T. Baine, S. Kudo, S. Tian, X. A. N. Ma, H. Zhou, N. J. DeYonker, T. C. Pham, J. C. Bollinger, D. L. Baker, B. Yan, C. E. Webster and X. Zhao, *Angew. Chem. Int. Ed.*, 2012, **51**, 5941-5944.
21. A. Call, Z. Codolà, F. Acuña-Parés and J. Lloret-Fillol, *Chem. Eur. J.*, 2014, **20**, 6171-6183.
22. T. Noji, M. Kondo, T. Jin, T. Yazawa, H. Osuka, Y. Higuchi, M. Nango, S. Itoh and T. Dewa, *J. Phys. Chem.*, 2014, **5**, 2402-2407.
23. O. A. Zadvornyy, J. E. Lucon, R. Gerlach, N. A. Zorin, T. Douglas, T. E. Elgren and J. W. Peters, *J. Inorg. Biochem.*, 2012, **106**, 151-155.
24. T. Sakai, D. Mersch and E. Reisner, *Angew. Chem. Int. Ed.*, 2013, **52**, 12313-12316.